Hindawi
Advances in Meteorology
Volume 2023, Article ID 1685720, 17 pages
https://doi.org/10.1155/2023/1685720

Research Article

Evaluation of Satellite Precipitation Products for Estimation of Floods in Data-Scarce Environment

Muhammad Masood,[1] **Muhammad Naveed**,[2] **Mudassar Iqbal**,[1] **Ghulam Nabi**,[1] **Hafiz Muhammad Kashif**,[1] **Muhammad Jawad**,[1] **and Ahmad Mujtaba**[1]

[1]*Centre of Excellence in Water Resources Engineering, University of Engineering & Technology GT-Road, Lahore 54890, Pakistan*
[2]*Department of Civil Engineering, University of Engineering & Technology GT-Road, Lahore 54890, Pakistan*

Correspondence should be addressed to Muhammad Masood; chmasoud@gmail.com

Received 22 November 2022; Revised 22 March 2023; Accepted 11 April 2023; Published 3 May 2023

Academic Editor: Tomeu Rigo

Utilization of satellite precipitation products (SPPs) for reliable flood modeling has become a necessity due to the scarcity of conventional gauging systems. Three high-resolution SPPs, i.e., Integrated Multi-satellite Retrieval for GPM (IMERG), Global Satellite Mapping of Precipitation (GSMaP), and Climate Hazards Group InfraRed Precipitation with Station (CHIRPS), data were assessed statistically and hydrologically in the sparsely gauged Chenab River basin of Pakistan. The consistency of rain gauge data was assessed by the double mass curve (DMC). The statistical metrics applied were probability of detection (POD), critical success index (CSI), false alarm ratio (FAR), correlation coefficient (CC), root mean square error (RMSE), and bias (B). The hydrologic evaluation was conducted with calibration and validation scenarios for the monsoon flooding season using the Integrated Flood Analysis System (IFAS) and flow duration curve (FDC). Sensitivity analysis was conducted using ±20% calibrating parameters. The rain gauge data have been found to be consistent with the higher coefficient of determination (R^2). The mean skill scores of GSMaP were superior to those of CHIRPS and IMERG. More bias was observed during the monsoon than during western disturbances. The most sensitive parameter was the base flow coefficient (AGD), with a high mean absolute sensitivity index value. During model calibration, good values of performance indicators, i.e., R^2, Nash–Sutcliffe efficiency (NSE), and percentage bias (PBIAS), were found for the used SPPs. For validation, GSMaP performed better with comparatively higher values of R^2 and NSE and a lower value of PBIAS. The FDC exhibited SPPs' excellent performance during 20% to 40% exceedance time.

1. Introduction

A flood is a frequently recurring destructive natural hazard that humanity encounters [1]. The adverse flooding conditions have resulted in a significant deterioration of environmental sustainability [2] throughout the world, wreaking havoc with costly infrastructure, food production, and human lives [3]. Globally, climate change and anthropogenic activities have increased the frequency and intensity of floods and exacerbated riverine flood threats in several world places [4]. Pakistan is located in a highly vulnerable region to climate change where floods occur almost every year since the last three decades [5, 6]. The devastating flood in Pakistan's history has emphasized the critical need for an efficacious and steadfast flood warning system [7]. Improved flood modeling and remote sensing necessitate enhanced flood analysis methodology to send timely warnings to populations and better reservoir operations [8]. The early warning system in Pakistan has limited capabilities. Although substantial improvements in flood forecasting have been made by utilizing the weather radar and telemetric systems in the warning system, there is still a need for many efforts to advance the flood forecasting and warning system [9, 10].

Precipitation is an important hydrological parameter used for watershed management, flood forecasting, and

climatological assessment [11]. It is also the most complex parameter because of its excessive spatiotemporal variations that traditional rain gauges and radar networks cannot record due to their sparsity [12]. Accurate and precise precipitation data with fine spatiotemporal resolution is important for watershed management and flood analysis [13]. It necessitates the need for such techniques that supplements the rain gauge observations and provides exceptional precipitation data to support hydrological modeling issues [14–16].

Remote sensing satellites use reflected light to detect, collect, measure, and record the electromagnetic energy from the earth's surface [17]. Advances in satellite remote sensing have made it an excellent data source, as it can provide metrological data to support hydrological modeling issues [18–20]. Moreover, precipitation data obtained from remote sensing have the potential to supplement the traditional rain gauge system [21].

Recent studies have shown that the precipitation data estimated through satellite-based observations contributed well to detecting rainfall distribution and severity in data-scarce regions [22, 23]. However, the satellite products may have errors due to indirect estimation, sampling uncertainty, and retrieval algorithms [24–27]. The properties of these errors significantly vary in contrasting climates, storms, seasons, and altitudes [11, 28]. Therefore, it is essential to validate the accuracy of satellite precipitation products and suitability for a broader range of environments. Satellite rainfall data can be validated using statistical analysis regarding ground-based on gauge data and a proper hydrological modeling framework [29]. Statistical analysis determines the accuracy and consistency of satellite precipitation data, while hydrological simulation elucidates the usefulness and application of the same datasets [30]. For reliable hydrological modeling, a proper calibration technique, parametric sensitivity, and model capability are of primary consideration. A suitable calibration technique is critical because errors in model calibration and input datasets contribute to incorrect outcomes [31]. Similarly, parametric sensitivity produces only important parameters, reduces the analysis time, and contributes to modeling calibration [32].

Furthermore, the ability of the hydrological model to simulate water flow can be examined using the FDC, "a key runoff variability signature" [33]. The FDC offers additional details on the basins' hydrological modeling and underlying processes [34, 35]. Generally, lumped, semidistributed, and distributed models are used for a watershed's hydrological modeling. Lumped models consider spatially uniform watershed characteristics. The semidistributed model divides the watershed into subbasins with unique hydrological responses [36]. Conversely, distributed models consider the spatial and temporal variation of physical properties in the watershed. These models can interpolate the rainfall data and predict water flow at ungauged locations. However, these models require a considerable input data set for flow estimations [37].

Recently, studies reported that statistical assessment of precipitation data had not yielded reliable results that necessitated hydrological modeling. In Pakistan, limited studies have been conducted to assess satellite precipitation products' effectiveness, particularly utilizing the distributed IFAS model. In [38], the authors highlighted the scarcity of hydrological data and the significance of upstream flow boundary conditions when barrage operation standards are unknown in the Indus River. In [31], the authors used a lump and regional calibration approach to model the Jhelum river basin. In [39], the authors pointed out the difficulty of flood modeling at the confluence point of the Chenab and Jhelum basins. In [38], the authors explored that the performance of IFAS can be improved by utilizing local soil texture data in the Indus River. In [38], the authors evaluated the precipitation results from different sources for modeling the Indus River's middle reach. Aziz [40] demonstrated that IFAS could be used for hydrological modeling of the Kabul River with data scarcity. In [41], the authors investigated that integrating satellite and gauge rainfall data can enhance flood forecasting in the Philippines-Cagayan River catchment. In [42], the authors recommended that improved satellite precipitation data be used to enhance flood prediction in the Dungun River basin, Malaysia.

Assessment of SPPs with a fully distributed hydrological model under different calibration scenarios is yet to be evaluated in the study area. In addition, the representation of hydrological signatures with different rainfall data sets is yet to be explored. It mandates the investigation of satellite precipitation data sets using a distributed hydrological model for different applications. In this study, three SPP-based datasets, i.e., IMERG, GSMaP, and CHIRPS, have been evaluated statistically and hydrologically in a data-scar region, i.e., the Chenab River catchment of Pakistan. The study utilized the IFAS model to generate streamflow for a sparsely gauged catchment by using satellite precipitation datasets and derived hydrological signatures.

2. Study Area and Data Description

2.1. Study Area. The Chenab River starts in Himachal Pradesh, India, at the confluence of the Bhaga and Chandra streams and flows across Indian-controlled Kashmir to Pakistan [43]. The catchment of the Chenab River covers an area of about 26,000 km^2 up to the Marala Barrage. It embraces 97% of this catchment area in India, while only 3% in Pakistan up to the Marala barrage [44]. In Pakistan, there are four streamflow gauge stations on the river, i.e., Marala barrage, Khanki barrage, Qadirabad barrage, and Trimmu barrage. For the present research, the study area ranged from the Marala barrage to the Trimmu barrage (Figure 1).

Since the Chenab River and Jhelum River converged at the Trimmu barrage, hydrological modeling at the convergence point is not possible [39]. So, the study considered the assessment of outflow at Qadir Abad barrage with an assumption of free flow at Khanki barrage during the monsoon flooding season. The selected catchment is situated between latitudes 72°–78° E and longitudes 32°–34° N, spanning over ~16,000 km^2, with a gradient of 0.4 m/km downstream of plain areas [43].

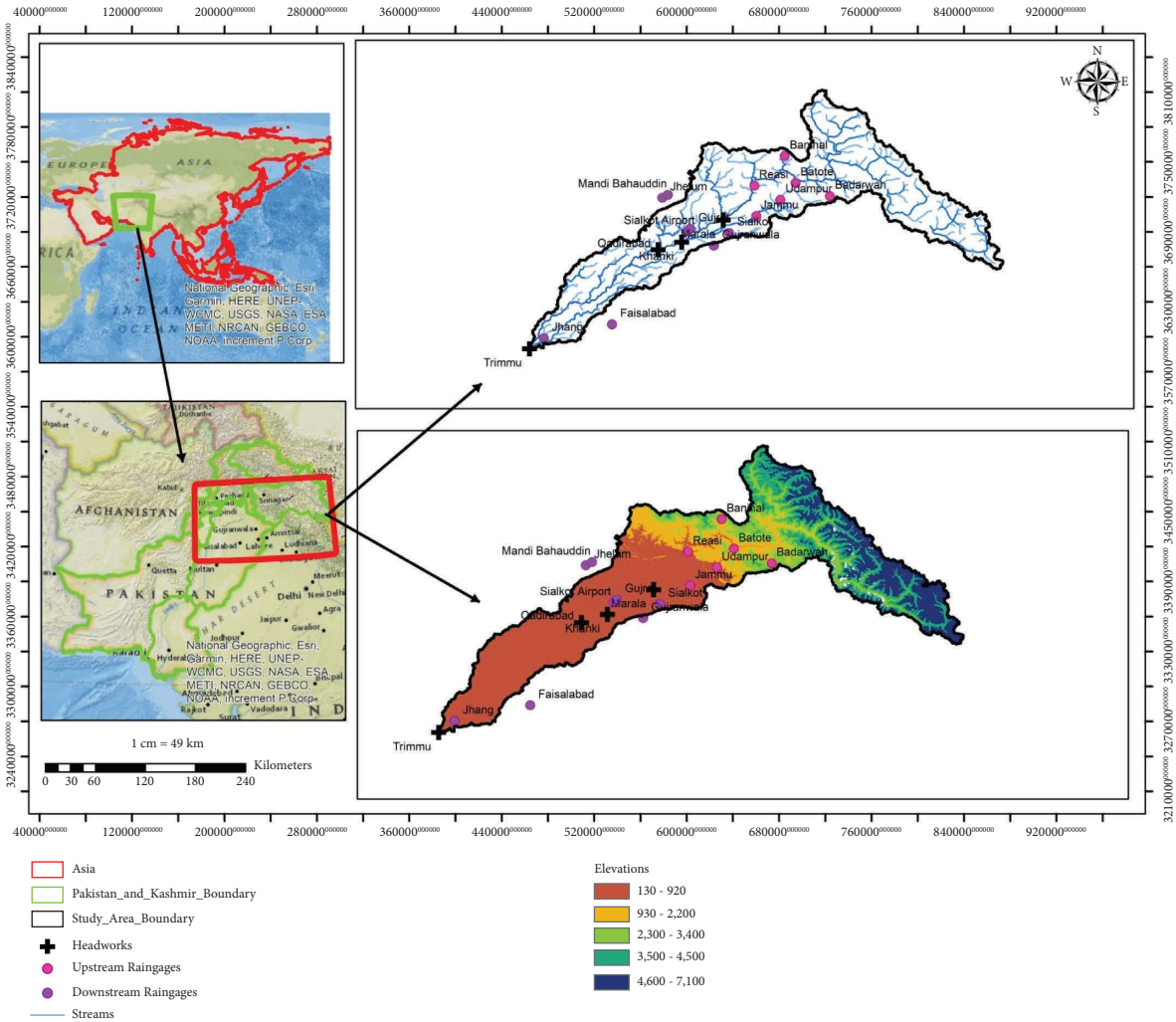

FIGURE 1: Location map of the Chenab River Basin showing catchment area, upstream and downstream gauging stations of Marala Barrage.

The crosssectional characteristics of the basin comprise 85 km in length with an average width of 800 m. The scarcity and sparsity of meteorological gauging stations are big concerns in this region. There are only four rain gauges organized by the Pakistan Meteorological Department (PMD), which do not meet the requirements of the World Meteorological Organization (WMO) and are inadequate for hydrological modeling for watershed management. The central hydrology of the catchment is controlled by the summer monsoon and winter seasons, where the summer monsoon season dominates and has triggered significant flooding in this region.

2.2. Data Description. The data for the research was collected at a daily scale for the years 2015–2020 and consisted of a gauge rainfall dataset, observed streamflow, and a satellite precipitation dataset. In addition, the topographical data comprises a digital elevation model, land use, and soil type. Daily rainfall data for the selected rain gauge stations were acquired from the PMD. Streamflow data for stream gauging stations were collected from Pakistan's Flood Forecasting Division (FFD).

Satellite precipitation datasets at the daily time scale (Table 1) consisting of GSMaP, IMERGE, and CHIRPS were downloaded from the Japan Aerospace Exploration Agency (JAXA) (https://sharaku.eorc.jaxa.jp/GSMaP/), National Aeronautics and Space Administration (NASA) (https://pmm.nasa.gov/data-access/downloads/gpm), and the University of California, Santa Barbara's Climate Hazards Group (UC Santa Barbara) (https://chg.geog.ucsb.edu/data/chirps/), respectively. GSMaP consists of four types of products; two real-time (GSMaP-NRT, GSMaP-Gauge, and NRT) and two postreal-time (GSMaP-Gauge, GSMaP-MVK). In the present work, GSMaP-Gauge NRT (version 6) was used. In order to formulate the GSMaP-Gauge NRT precipitation predictions with a 4 h latency period, the error parameters estimated for the postreal-time product of GSMaP-Gauge are utilized. GSMaP-Gauge also employed a blending of passive microwave (PMW) and infrared (IR) data along with a unified gauge-based analysis of the global daily precipitation dataset from the Climate Prediction Center (CPC) [22].

Table 1: Specifications of the three SPPs used in the study.

Specification	Satellite precipitation datasets		
	GSMaP	IMERG	CHIRPS
Developer	JAXA	NASA	USGS and CHC
Spatial resolution	0.1°	0.1°	0.05°
Temporal resolution	Daily	Daily	Daily
Coverage	60 N-60 S	90 N-90 S	50 N-50 S
Data availability	2014-onwards	2014-onwards	1981-onwards
Latency	4 hours	14 hours	48 hours
Frequency	1 hour	0.5 hour	24 hours
Algorithm	PMW and IR	GMI and DPR	CCD and gauge
Version	6	6	2

Similarly, Global Precipitation Measurement (GPM) is a multinational satellite project to integrate and enhance precipitation observations from different satellites. IMERG is a GPM-based level 3 multisatellite precipitation algorithm that incorporates all passive microwave and infrared-based observations in the constellation. Typically, three products of IMERG precipitation (early-run, late-run, and final-run) are mostly considered. Early-run uses only forward morphing with a 4 hour latency period; however, late-run and final-run use forward and backward morphing with latency periods of 14 hours and 3.5 months, respectively [45]. IMERG combines passive microwave, propagated pulse width modulation, and infrared radiation-based observations by the Kalman filter method to obtain precise estimation [46]. This research work utilized daily IMERG-late-run version 6 for statistical and hydrological assessments in the study area.

Moreover, CHIRPS is a quasi-global rainfall dataset that consists of three types of temporal data (daily, pentanal (5 days), and monthly) with two types of spatial resolution (0.05°, 0.25°). The daily data are considered real-time data with a latency period of 2 days, while pentanal and monthly data are considered post-real-time datasets with a 21 days latency period. Its algorithm is based on cold cloud duration (CCD) and ground gauge observations to approximate the rainfall. This study employed the daily 0.05° grid CHIRPS version 2.0 dataset [47].

Furthermore, digital elevation model (DEM) was used to represent the catchment's topography and delineate the watershed. The present study collected DEM and Global Map's land cover data (Version 2) from the International Steering Committee for Global Mapping (ISCGM). Finally, the soil type data based on the Digital Soil Map of the World (DSMW), provided by the Food and Agriculture Organization (FAO), was used.

3. Research Methodology

3.1. Double Mass Curve Analysis. DMC is employed to inspect the consistency of the hydrologic data and to adjust the inconsistent precipitation data. In this graphical approach, the cumulative data of a single station is compared with the pattern composed of cumulative data from other stations in the area. Likewise, for the used pattern, enough gauging stations must be included while checking the consistency of precipitation records so that inconsistency does not significantly influence the average in one of the station' records. If there are less than 10 stations located in a specific region, the consistency of each station must be examined. Therefore, at all four gauging stations located in the study area, the DMC technique was applied to examine the consistency of annual rainfall data.

3.2. Evaluation Statistics. The efficacy of selected satellite precipitation products was assessed against four-gauge station records with categorical and continuous metrics on a daily, ten daily, monthly, and seasonal scales from 2015 to 2020. Different approaches have been used by comparing point precipitation data observed by rain gauges with pixel precipitation data recorded by remote sensing satellites. Usually, such procedures are based upon the upscale interpolation of point values to grid scale data and the downscaling of grid data towards point values. The reanalyzed gridded data always vary from the station observations and vice versa in several aspects. To avoid inaccuracies caused by such upscale interpolation methods and downscaling, a more direct approach has been proposed and used. In this approach, precipitation observed at stations falling within a grid cell will be averaged to obtain an estimate for the observed precipitation at the center of that grid cell and then compared to the gridded value [21]. This approach has been used in this study for comparison between rain gauge and satellite data sets. For this purpose, satellite precipitation data at the daily time scale was downloaded and then converted into ten daily, monthly, and seasonal scales. In selecting the tile of satellite precipitation data, PMD gauge value recording time (8:00 am daily) was kept in focus. Event detection capability was evaluated with categorical metrics that include POD, FAR, and CSI. POD reflects the ratio of accurately identified rainfall events by the satellite concerning gauge rainfall data. FAR demonstrates the fraction of rainfall events in which the satellite predicts precipitation while the rain gauge does not observe it. CSI represents typically the fraction of rainfall occurrence accurately recognized by the satellite. Continuous metrics measure the quantitative difference between observed and predicted precipitation. These metrics include bias, CC, and RMSE. Bias is the mean discrepancy between satellite estimation and rain gauge data. Depending on the quality of the rainfall data, its value could be positive or negative, indicating

overestimation and underestimation, respectively. CC estimates the degree of agreement between the satellite and rain gauge precipitation data. RMSE depicts the mean dispersion of predicted precipitation around the known value of gauge observations. It is used to evaluate the precision of the rainfall dataset [48]. From historical data, two rainy seasons, monsoon (June to September) and westerly disturbance (November to February), have been established in the study area: these were considered for seasonal evaluation at the daily scale. These statistical metrics are given as follows:

$$\begin{aligned}
\mathrm{POD} &= \frac{H}{H+M},\\
\mathrm{FAR} &= \frac{F}{H+F},\\
\mathrm{CSI} &= \frac{H}{H+M+F},\\
\mathrm{BIAS} &= \frac{\sum_{i=1}^{n}(\mathrm{Si}-\mathrm{Gi})}{N},\\
\mathrm{RMSE} &= \sqrt{\frac{\left(\sum_{i=1}^{n}(\mathrm{Si}-\mathrm{Gi}).^{2}\right.}{N}},\\
\mathrm{CC} &= \frac{\sum_{I=1}^{n}(\mathrm{Gi}-\mathrm{Gm})(\mathrm{Si}-\mathrm{Sm})}{\sqrt{\sum_{i=1}^{n}(\mathrm{Gi}-\mathrm{Gm}).^{2}}\sqrt{\sum_{i=1}^{n}(\mathrm{Si}-\mathrm{Sm}).^{2}}},
\end{aligned} \tag{1}$$

where H, M, and F exhibit the number of hit, miss, and false alarm events, while Gi and Si denote the gauge and satellite precipitation, Gm and Sm represent the mean of gauge and satellite precipitation data, and N indicates the total number of events used for evaluation.

3.3. Explication of Hydrological (IFAS) Model. IFAS is a succinct runoff analysis toolkit designed for flood prediction in basins with insufficient hydrological and geophysical information in developing countries. It is categorized as a physically distributed framework that can integrate gauge rainfall data, satellite-based precipitation data, evaporation data, snowmelt data, and geophysical data to simulate river course flow. It integrates grid-based datasets of topography, geology, and land cover to estimate the parameters of the physical conditions of a basin [49]. The model can generate the channel network using topographical data to define the basin, sub-basin boundaries, flow direction, and drainage patterns. It employs the Public Works Research Institute Distributed Hydrological Model (PWRI-DHM), consisting of a two- or three-tank structure and a routing model for runoff simulation. The three-tank structure comprises a surface, sub surface, and aquifer, while the routing model comprises a kinematic hydraulic river course routing tank. PWRI-DHM uses a nonlinear relationship to calculate each cell's outflow based on the tank model philosophy, considering Manning's equation, Darcy's law, and hyperbolic approximations. It uses a kinematic wave equation to calculate the discharge in the river course tank [38, 50, 51].

3.4. Model Formulation. For the development of the IFAS model, the extent of the target study area was defined by determining the latitude and longitude of the selected catchment. The IFAS model with a two-layered and three-tank structure was created by customizing the digital-based land cover, elevation, and soil type data to the appropriate grid size. The shapefile of the study area was imported into the basin manager function of IFAS to define basin and sub basin boundaries. The surface tank parameters were estimated utilizing the land cover data, while the aquifer tank parameters were tuned according to soil type data. The essential aspect of hydrological modeling in a basin is accurately estimating runoff and water level initial conditions in the river course that affect the parameter optimization of the model [31]. The model was run six months before the calibration of the flood event to generate proper initial conditions until hydrological equilibrium was achieved. The principle of equifinality dictates that many combinations of parameters are possible that give good agreement with the observed streamflow data. Boundary conditions are essential, especially when hydrological data is scarce and standards for barrage operations are unknown. IFAS has an integrated water resources management (IWRM) interface that contains various techniques to incorporate barrage operating tasks. The discharge file technique was applied using the IWRM function to give the boundary condition in this study condition. This technique employed daily discharge data in the CSV file to represent barrage operations. Marala barrage outflows were considered boundary conditions in this research due to data scarcity and unknown barrage operations upstream of the catchment.

3.5. Calibration Scenarios and Model Performance Indicators. Since the outputs of hydrological models are rarely capable of accurately reflecting nature in its completeness, their performance must be evaluated before they can be employed in any decision-making process. The IFAS is designed for flood analysis; therefore, it was calibrated and validated utilizing precipitation data collected during the monsoon seasons (July to October) of 2015 and 2017, considering medium and high flooding years, respectively (PMD/FFD). The model was calibrated individually using CHIRPS, GSMaP, and IMERG precipitation datasets. All datasets were validated against each calibration scenario. The calibration of the model was achieved through a trial-and-error process. The model performance was evaluated using model performance indicators (MPI), R^2, NSE, and PBIAS. The R^2 is a statistical indicator representing the fraction of the dependent variable's variance predicted by the independent variable. The ideal value is 1, while a lower value than 1 reveals the variation of model output. The model performance with $R^2 > 0.5$ is acceptable. Likewise, the NSE is the most often used method for determining correlation to test the efficacy of hydrological models. The literature reveals a variety of acceptable, very good, and excellent value categories for NSE. The calibration tolerance criteria are very subjective. Calibration with NSE is generally perceived as good if it is higher than 0.6 and excellent if it is more

significant than 0.8 in the literature. The model validation criteria are less restrictive than the calibration levels. A value of NSE greater than 0.5 is acceptable for validation, while NSE greater than 0.7 is considered highly excellent. The PBIAS examines the average tendency of the simulated flows to be greater or smaller than their observed flows. The perfect value of PBIAS is 0, and lower values represent accurate model reproduction [52].

These MPIS are given as follows:

$$R^2 = \frac{\sum_{I=1}^{n} (\mathrm{Oi} - \mathrm{Om})(\mathrm{Pi} - \mathrm{Pm})}{\sqrt{\sum_{i=1}^{n} (\mathrm{Oi} - \mathrm{Om})} \sqrt{\sum_{i=1}^{n} (\mathrm{Pi} - \mathrm{Pm})}},$$

$$\mathrm{NSE} = 1 - \frac{\sum_{i=1}^{n} (\mathrm{Oi} - \mathrm{Pi}).^2}{\sum_{i=1}^{n} (0i - \mathrm{Om}).^2}, \tag{2}$$

$$\mathrm{PBIAS} = 100 * \frac{\sum_{i=1}^{n} (\mathrm{Oi} - \mathrm{Pi})}{\sum_{i=1}^{n} (0i)},$$

where Oi and Pi represent the observed and simulated flows, Om and Pm are denoted by the mean values of the observed and simulated flows, and n is the total number of events.

3.6. Implications of Sensitivity Analysis Technique. The sensitivity analysis helps to examine the nonlinear variation of highly uncertain parameters in the complex models. The IFAS model was investigated to determine the most sensitive calibrating parameters severely affecting the calibrating hydrograph. In this regard, the values of all calibrated parameters were first increased and then decreased by 20%, one by one of their calibrated values. $C_{+20\%}$ is the 20 percent change in the calibrated parameter value and is determined using equation (3). So are the simulation results of a calibrated hydrograph, and $S_{+20\%}$ is the change that occurred in the simulation results when one of the calibrating parameters' values changed to +20%. The mean percentage change in the simulation results by increasing or decreasing the calibrating parameter value to 20% is called the sensitivity index (I) and can be determined using equation (4). The mean absolute sensitivity index (MASI) can be determined using equation (5).

$$C_{\pm 20\%} = \left\{ \frac{(S_0 - S_{\pm 20})}{S_0} \right\} \times 100, \tag{3}$$

$$I_{\pm 20\%} = \frac{(C_+ + C_{-20})}{2}, \tag{4}$$

$$\mathrm{MASI} = \frac{\left\{ \left| C_{+20} \right| + \left| C_{-20} \right| \right\}}{2}. \tag{5}$$

3.7. Flow Assessment Using Hydrological Signature. The FDC is an influential streamflow variability signature that describes hydrological behavior. It is the graphical representation of flows and the percentage of time that the flows equal or surpass each other. Satellite precipitation datasets were evaluated through the FDC, in which the observed streamflow was taken as the baseline and the variation in simulated flow was evaluated. Furthermore, the ability of each precipitation dataset to generate high and medium flows was examined through dependable flow exceedance, where the extreme flood events were represented in the range of Q5–Q25 dependable flows, the medium flow required for irrigation was designated by Q50 dependable flows, and Q70 dependable flows correspond to the water availability for domestic supply.

4. Results and Discussion

4.1. Consistency of Gauge Rainfall Data. Double mass analysis has been used to check the consistency of rainfall data records at four stations, i.e., Gujrat, Sialkot, Sargodha, and Jhang. The cumulative data of a single station was compared with the cumulative data of other stations in the respective area.

The straight line shows data consistency, whereas any change in the straight line manifests a change in the data collection method that affects the relationship. For any station, the rise of the curve from the trend line shows that there was more annual rainfall than in other stations. For all gauging stations, the R^2 values were 0.98 to 0.99, and the annual rainfall data were consistent with the DMC technique (Figure 2). where CAR = is the cumulative annual rainfall.

4.2. Statistical Evaluation of SPPs at Different Temporal Scales. This study identified and quantified the errors associated with satellite datasets. The efficacy of selected satellite products (CHIRPS, IMERG, and GSMaP) was assessed statistically at daily, 10-daily, monthly, annual, and seasonal scales using precipitation data recorded at PMD stations.

4.2.1. Daily and 10-Daily Scale. Statistical evaluations of selected SPPs at daily and 10-daily levels are presented in Table 2. In the case of categorical metrics, the mean POD of GSMaP was better than CHIRPS and IMERG on both temporal scales. The mean POD for CHIRPS and IMERG was lower by 50.79% and 22.22% for the daily scale with reference to GSMaP. In terms of mean FAR values, IMERG and GSMaP showed good agreement, and CHIRPS underperformed. CSI gives more stable results due to the characteristics of the blending of POD and FAR. The performance of GSMaP, IMERG, and CHIRPS was improved by 54%, 58%, and 55%, respectively, for CSI at the 10-daily scale. Remarkably better values of categorical metrics were given by all the used satellite products at the 10 daily time scale as compared to the daily time scale.

In the case of continuous metrics, the mean BIAS of GSMaP was better than the other two products at daily scale. A slight difference was observed between the mean RMSE values of the selected products on both temporal scales. However, it was noted that the used SPPs showed less errors (BIAS and RMSE) on a daily scale, compared to 10 daily. Probably this was due to a reduction in sample size at a larger time scale as compared to a smaller time scale. All SPPs did not show good agreement with rain gauge data at the daily

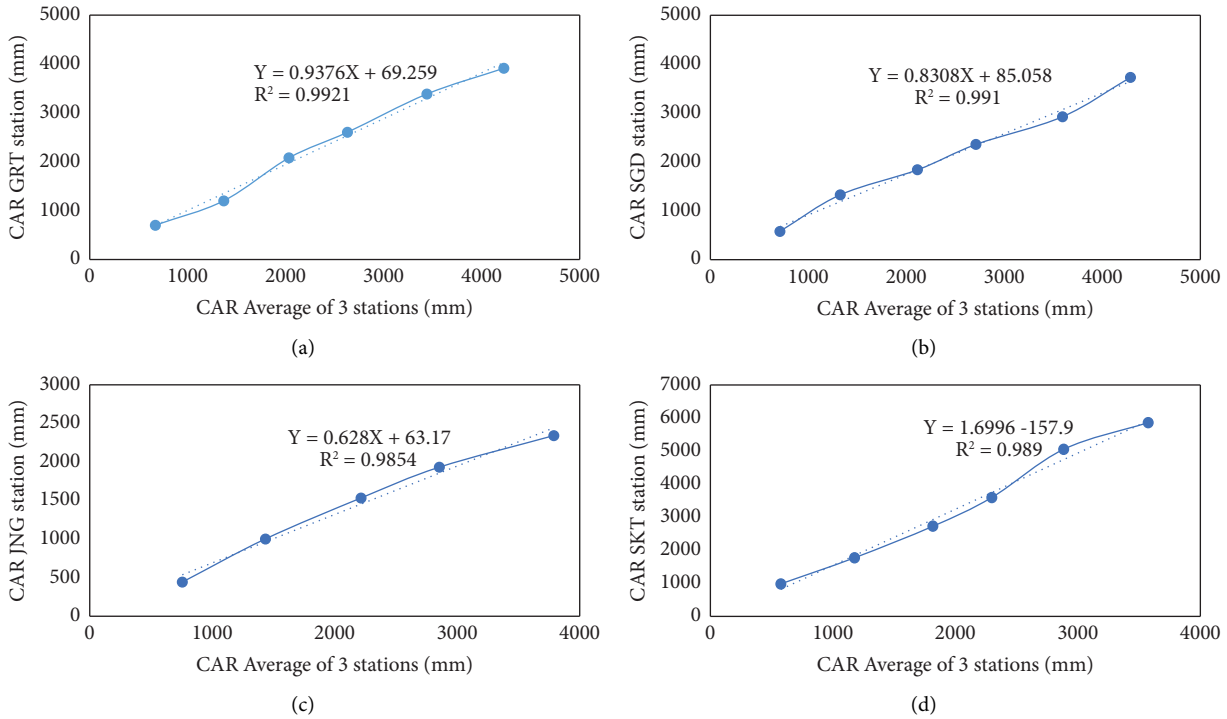

Figure 2: Consistency assessment of rain gauge data in the study area based on DMA. (a) Gujrat (GRT) Gauge Station. (b) Sargodha (SGD) Gauge Station. (c) Jhang (JNG) Gauge Station. (d) Sialkot (SKT) Gauge Station.

Table 2: Evaluation of the used SPPs based on mean values of categorical and continuous metrics at daily and 10-daily time scales.

Assessment scale	Satellite product	Categorical metrics			Continuous metrics		
		POD	FAR	CSI	BIAS (mm)	RMSE (mm)	CC
Daily scale	GSMaP	0.63	0.63	0.29	0.13	8.32	0.3
	CHIRPS	0.31	0.74	0.17	0.44	9.24	0.21
	IMERG	0.49	0.68	0.24	0.08	9.57	0.25
10-daily scale	GSMaP	0.97	0.14	0.83	1.3	23.75	0.71
	CHIRPS	0.86	0.18	0.72	0.99	27.55	0.62
	IMERG	0.97	0.16	0.82	4.42	23.35	0.74

scale. The correlation coefficient was low at 0.21–0.30 at the daily scale, while it was high at 0.71–0.74 at the 10-daily scale, showing better performance of SPPs at a larger time scale, identical with categorical metrics. Overall, the statistical performance of SPPs was lower on a daily scale and higher on a 10-daily scale.

4.2.2. Monthly and Annual Scale. Figure 3 shows a monthly comparison of IMERG, GSMaP, and CHIRPS precipitation observations with the reference data for the entire study period (January 2015 to December 2020). The GSMaP precipitation product represented the best monthly precipitation temporal pattern. However, both IMERG and CHIRPS were also capable of representing the temporal variability of observed precipitation over the study area, albeit with notable overestimation. In July and August of 2016, 2017, and 2018, all precipitation data sources (gauges, IMERG, GSMaP, and CHIRPS) revealed increased precipitation magnitude. Almost all data sources exhibited a similar temporal pattern in monthly estimates from January to December 2015. All SPPs significantly overestimated precipitation for July through September 2020.

On an annual time scale, a comparison was made between the rain gauge values and the used SPP values shown in Figure 4. The annual average precipitation in the study area, as estimated from observations from 2015 to 2020 from four gauging stations, was 691 mm/year. It has been observed that the selected satellite-based precipitation products overestimated the annual precipitation amounts. IMERG and GSMaP showed overestimations of 23.47% and 7.17%, respectively, while CHIRPS showed an overestimation of 1.08% with reference to rain gauge values.

The result showed some difference in estimating precipitation magnitudes by the IMERG products over the Chenab River basin of Pakistan, but the performance of CHIRPS and GSMaP encourages the utilization of SPPs in the study area at an annual time scale. Several researchers have also reported identical findings in different regions of the world.

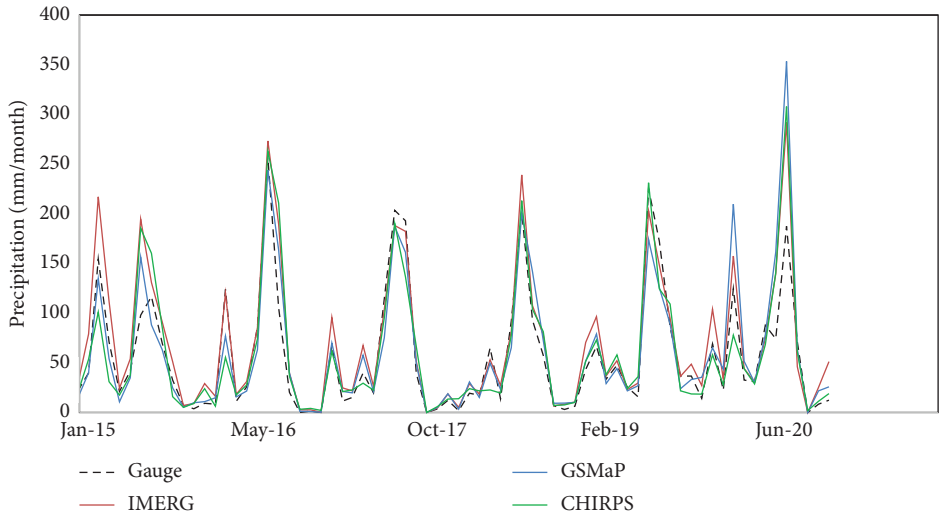

Figure 3: Comparison among precipitation estimates by the PMD gauges and the three SPPs at the monthly time scale in the study area.

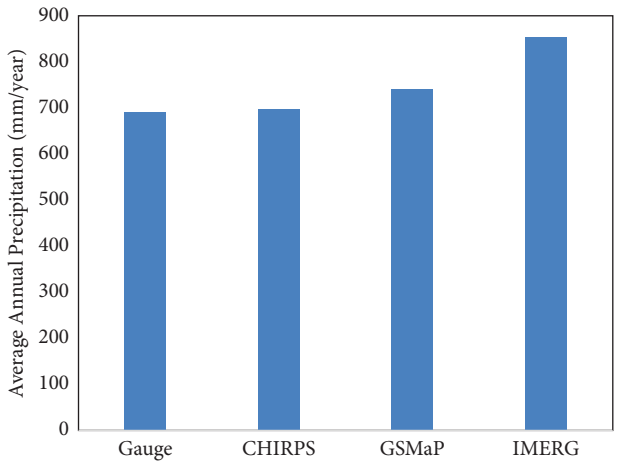

Figure 4: Comparison among average annual precipitation estimated by the PMD gauges and the three SPPs in the study area.

4.3. Evaluation of SPPs at the Seasonal Scale

4.3.1. Summer Monsoon Season. Figure 5 shows the performance of SPPs through box plots during the monsoon season for the study period. The categorical detection indices revealed that POD results were found in the range of 0.26 to 0.85. The precipitation detection capability of GSMaP was better with a POD of 0.75, followed by IMERG and CHIRPS with values of 0.56 and 0.34, respectively. Notably, all SPPs revealed large FAR values during the monsoon season. The performance of the selected SPPs was lower in terms of CSI. Inter comparing the results of CSI revealed the better performance of GSMaP for the monsoon period. In the case of bias, an agreement was observed between CHIRPS and IMERG, while GSMaP revealed better performance. The results of RMSE indicated that the first quartile of daily data was found in the range of 11 to 20 mm per day for the selected three products. The values of the second and third quartiles of RMSE were observed at about 11 to 17 mm/day. For the CC results, it was observed that the median values varied from 0.21, 27, and 0.29 for CHIRPS, IMERG, and GSMaP, respectively. Intercomparing between SPP revealed that GSMaP depicted higher values of CC. The statistical performance in terms of BIAS, RMSE, and CC of the selected products revealed that the overall efficiency of GSMaP has remained higher than the other two products in the monsoon season.

4.3.2. Winter Western Disturbance Season. Figure 6 shows the performance of SPPs towards estimation of precipitation during winter due to the western disturbance season (westerly waves) for the entire study period based on daily precipitation data. The event detection capability revealed that the POD of GSMaP was higher and better than the other two products. The CHIRPS underperformed in terms of POD values. In the case of FAR, GSMaP outerperformed than IMERG and CHIRPS. In the case of CSI, all selected SPPs revealed better performance during western disturbances. In the case of bias value, IMERG overestimated the precipitation, while CHIRPS showed excellent performance. While considering the results of RMSE, an agreement was observed between the median values of CHIRPS and GSMaP. The box plot results showed the RMSE values ranged from 2.5 to 7.5 mm/day for the selected satellite products, and higher values were produced by the IMERG. A strong agreement between CHIRPS and IMERG was observed for the CC results. Intercomparison revealed that SPPs showed comparatively better statistical performance during western disturbance than monsoon season.

Conclusively, the statistical performance of GSMaP is better than other SPPs, as also reported in [22, 53, 54], in other regions of the world.

4.4. Parametric Sensitivity Assessment. Figure 7 shows the sensitivity analysis of the IFAS model for surface, aquifer, and river course tank parameters based on the mean absolute sensitivity index (MASI). In the case of surface tank parameters, the surface tank height (HFMND) and final

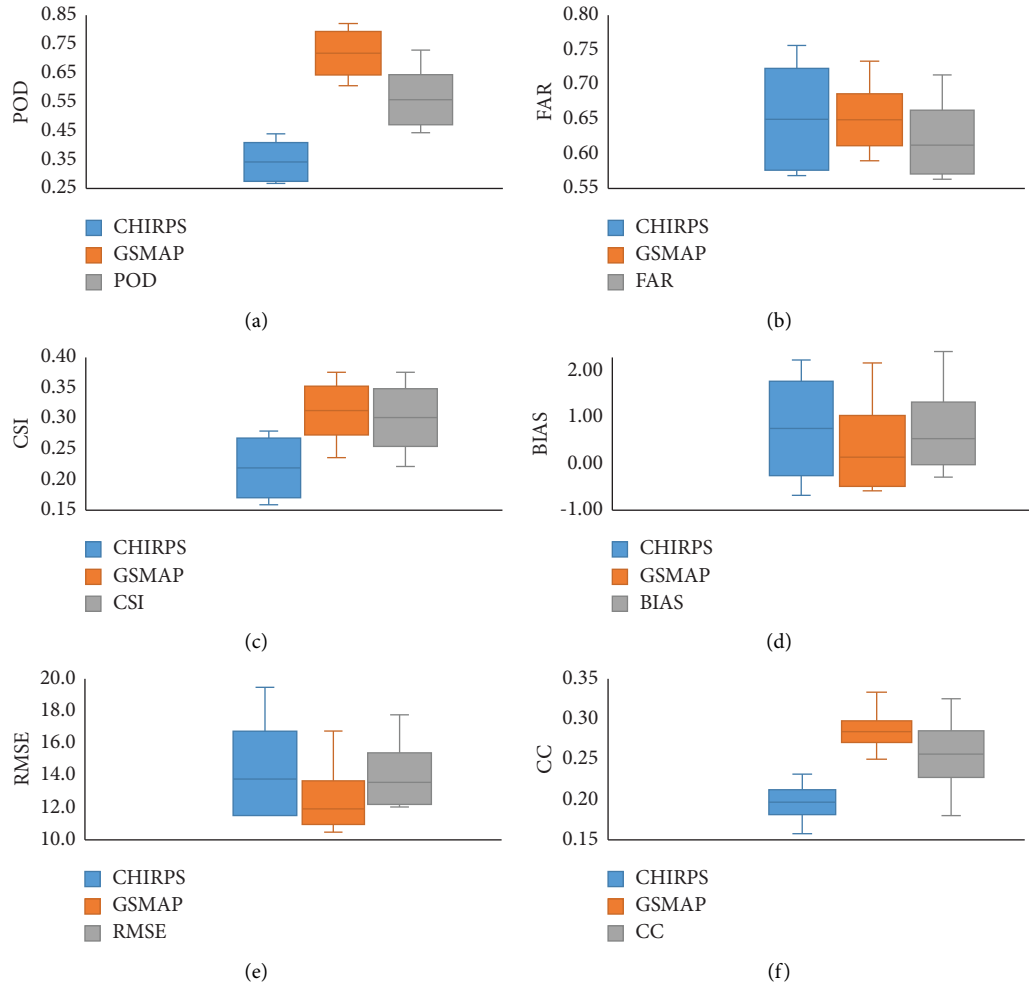

Figure 5: Statistical (continuous and categorical) assessment results of the used SPPs at a seasonal scale during the summer monsoon period. (a) POD. (b) FAR. (c) CSI. (d) BIAS. (e) RMSE. (f) CC.

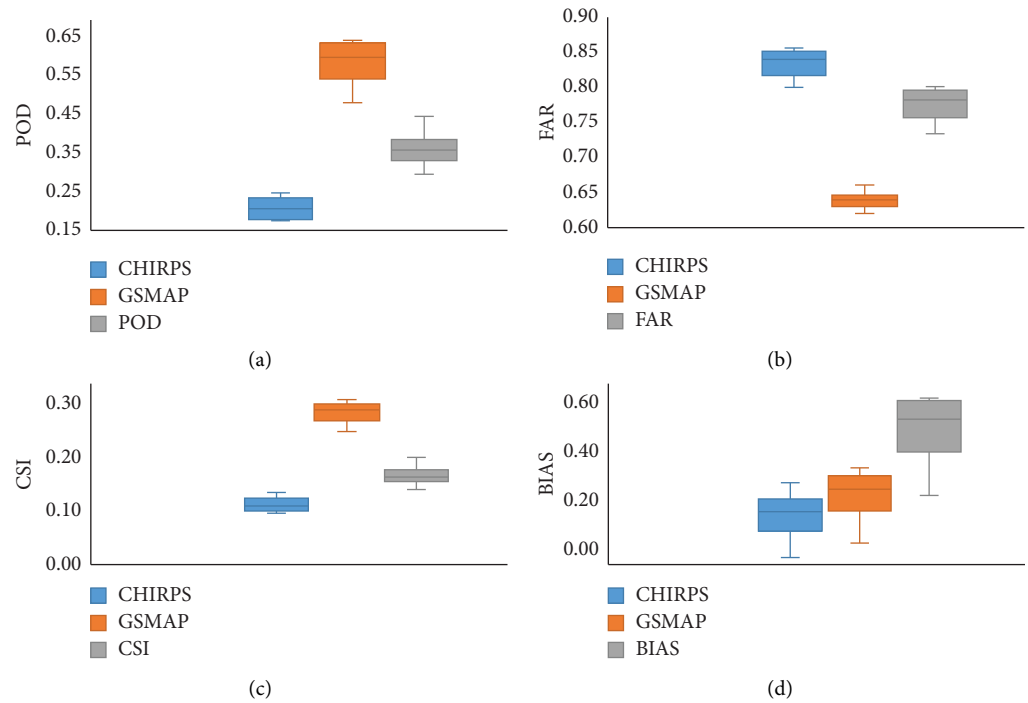

Figure 6: Continued.

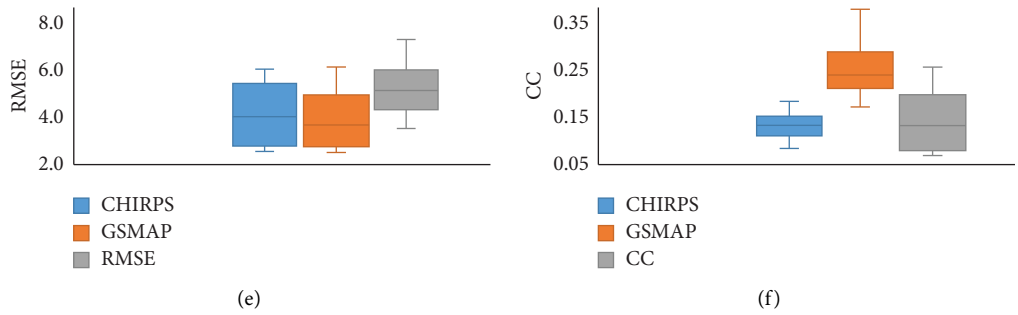

Figure 6: Statistical (continuous and categorical) assessment results of the used SPPs at seasonal scale during the winter westerly wave period. (a) POD. (b) FAR. (c) CSI. (d) BIAS. (e) RMSE. (f) CC.

infiltration capacity of soil (SKF) are the most sensitive parameters, with a mean absolute sensitivity index (MASI) of 8 and 3.5, respectively. It was observed that other surface tank parameters, i.e., SNF, HFOD, and HFID, do not significantly impact the calibration of the model and show a lower mean absolute sensitivity index. Similarly, the evaluation of aquifer tank parameters indicated that the parameters, i.e., the effect of storage height to generate base flow (AGD) and the initial value used for calculation (HIGD), are the two most sensitive parameters, with MASI values of 452 and 99, respectively. The aquifer parameter HIGD depicted a direct relationship with the change in simulation results of the hydrograph, while HCGD and AUD do not influence the calibration of the model.

Meanwhile, the analysis of the river course tank parameters indicated that the parameters related to the coefficients of a crosssection of a river, i.e., RLCOF and RBS, were sensitive to the simulated hydrograph. The aquifer tank parameters are more sensitive than any other tank parameters also reported by [55], and river tank parameters played significantly less in calibration. Therefore, it is suggested to introduce the option of actual groundwater conditions in the IFAS model for the target area.

The IFAS model was calibrated and validated for the river Chenab at Qadir Abad barrage outlet for the monsoon periods of 2015 and 2017, respectively, utilizing the selected SPPs. In the calibration process, initially the default parameters for surface and aquifer tanks were used to run the model. The surface parameters were based on digital land cover data, while the aquifer parameters were based on soil type data for the selected basin. The parameters were tuned and optimized with the trial-and-error technique to bring them into sound agreement with the observed flow data. The critical parameters considered for a successful calibration of the model are the coefficient of base flow regulation (AGD) for the aquifer tank, the surface tank height (HFMND), the final infiltration capacity of the soil (SKF), and the initial height of infiltration (HFOD) for the surface tank. Since HFOD is a surface parameter, it significantly influences the adjustment of the peak of the hydrograph. Due to the surface tank's five distinct feature classes, successful peak calibration requires fine-tuning of the land cover parameter. Land cover classes from the IFAS graphical module were used to calibrate the model, which was then fine-tuned using a trial-and-error method. Another surface tank parameter (FALFX) was tuned from 0 to 1 to control the subsurface flow to calibrate the model. The values of FALFX parameters were subsequently decreased to adjust the hydrograph in the calibration process.

Three different calibration scenarios were established to investigate the capacity of selected SPPs to calibrate the IFAS model and to examine their effectiveness for different applications. In the first scenario, the model was calibrated utilizing the CHIRPS satellite precipitation data, and then the validation process was completed using the GSMaP and IMERG. For the second scenario, the IFAS model was calibrated utilizing the GSMaP, and the model was validated by using CHIRPS and IMERG for evaluation. In the third scenario, the IMERG precipitation dataset was utilized to calibrate the IFAS model and then validated against GSMaP and CHIRPS. Calibration and validation of the IFAS model were evaluated using the model performance indicators, i.e., NSE, R2, and PBIAS. The model's performance on each scenario and comparison among the performance of the three scenarios are presented in Table 3.

For the first calibration scenario, the statistical performance indicators R^2, NSE, and PBIAS were 0.89, 0.86, and −0.16, respectively. The intercomparison results of model validation for this scenario revealed the better performance of the GSMaP dataset with R^2, NSE, and PBIAS values of 0.85, 0.83, and 0.16, respectively. The IMERG and CHIRPS datasets showed slightly lower performance during the model validation process. From the graphical presentation of scenario 1 in Figure 8, some variations in simulating low and high flows were observed by the SPPs.

For the second calibration scenario, the statistical performance indicators (R^2, NSE, and PBIAS) were 0.97, 0.96, and −0.03, respectively. According to the calibration criteria, this scenario displayed excellent performance, demonstrating that GSMaP precipitation data resulted in a robust and trustworthy testing model with utility and accuracy that could be used to check and compare the results produced from the IMERG and CHIRPS precipitation models. Comparison of model validation results revealed that the GSMaP dataset outperformed the other datasets, with R^2, NSE, and PBIAS values of 0.9, 0.89, and 0.14, respectively. A strong agreement was observed between IMERG and CHIRPS-based simulated flows. The ability of the GSMaP

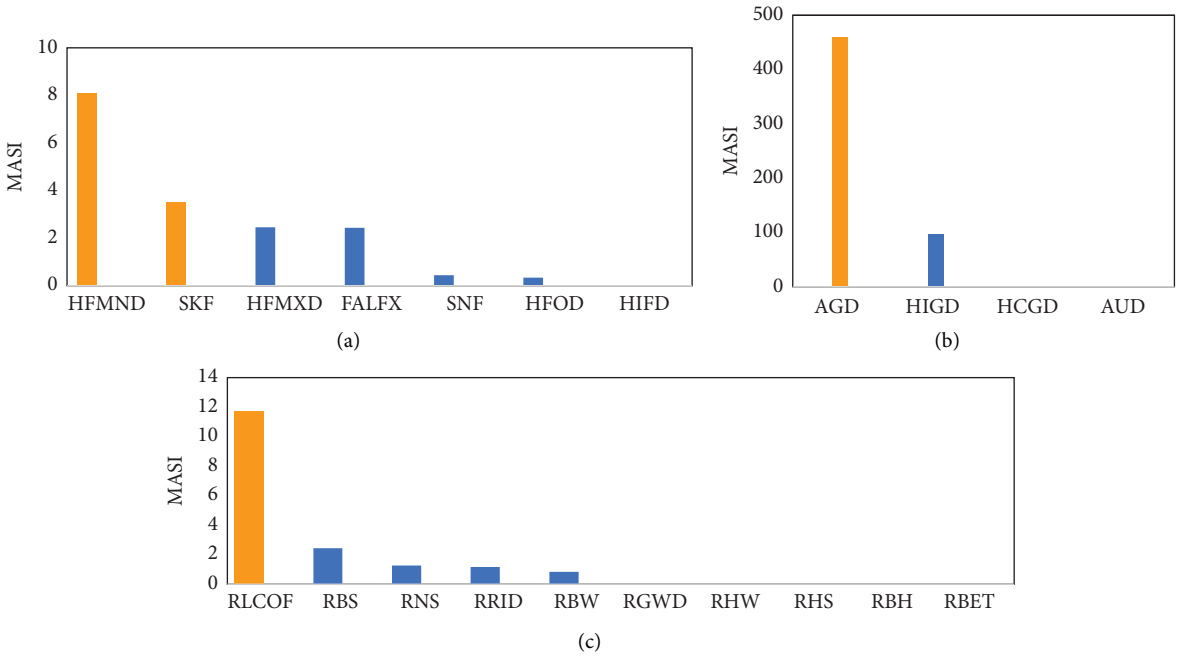

Figure 7: Sensitivity assessments among various parameters of the IFAS model. (a) Surface parameters. (b) Aquifer parameters. (c) River course parameters.

Table 3: Performance evaluation comparison among the used calibration and validation scenarios.

Year	Scenario 1 CHIRPS rainfall model				Scenario 2 GSMaP rainfall model				Scenario 3 IMERG rainfall model			
	SPP	NSE	PBIAS	R^2	SPP	NSE	PBIAS	R^2	SPP	NSE	PBIAS	R^2
Calibrated 2015	CHIRPS	0.86	−0.16	0.89	GSMaP	0.96	−0.03	0.97	IMERG	0.91	−0.11	0.92
Validated 2017	CHIRPS	0.78	0.17	0.83	GSMaP	0.80	0.25	0.89	CHIRPS	0.80	0.17	0.85
Validated 2017	GSMaP	0.80	0.16	0.84	IMERG	0.78	0.16	0.84	GSMaP	0.82	0.16	0.86
Validated 2017	IMERG	0.79	0.15	0.82	CHIRPS	0.77	0.26	0.88	IMERG	0.81	0.16	0.85

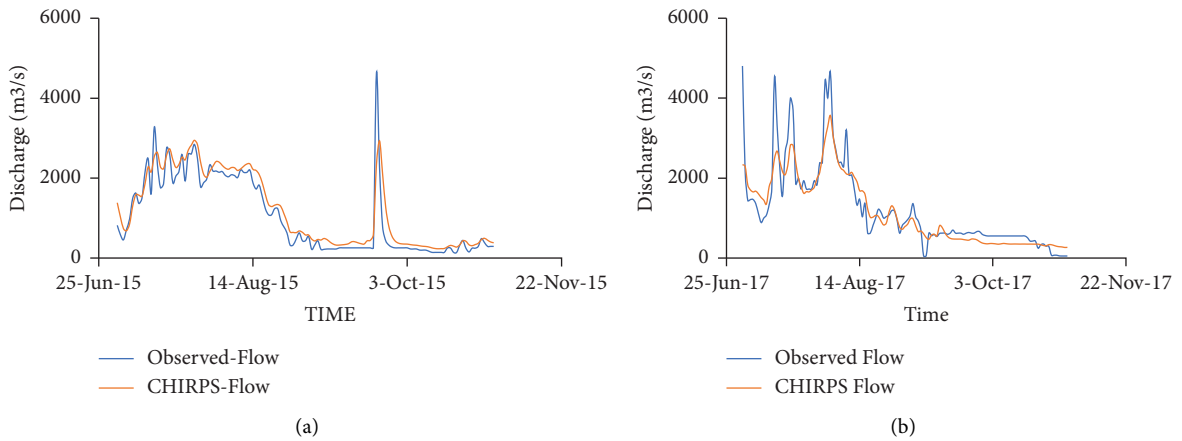

Figure 8: Continued.

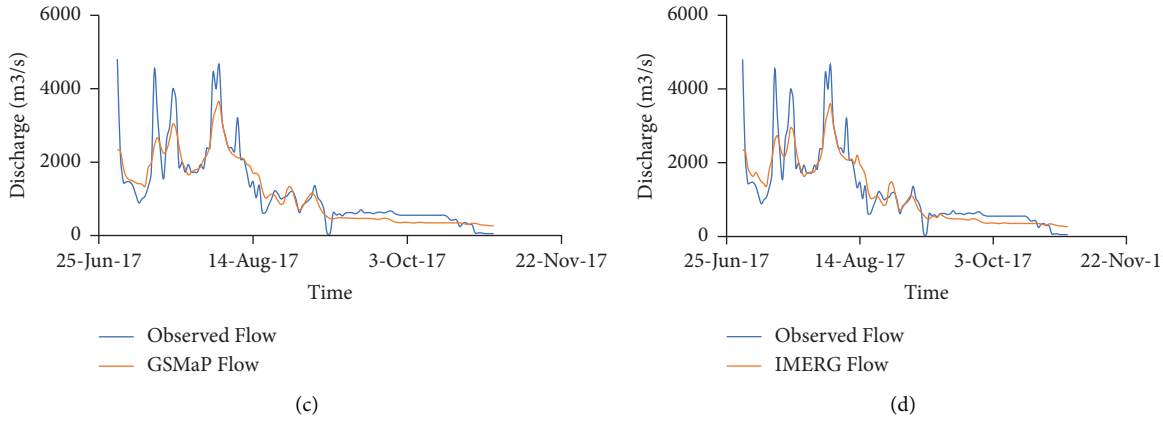

Figure 8: Graphical representations of calibration and validation scenario 1. (a) Calibration-CHIRP. (b) Validation CHIRPS. (c) Validation GSMaP. (d) Validation IMERG.

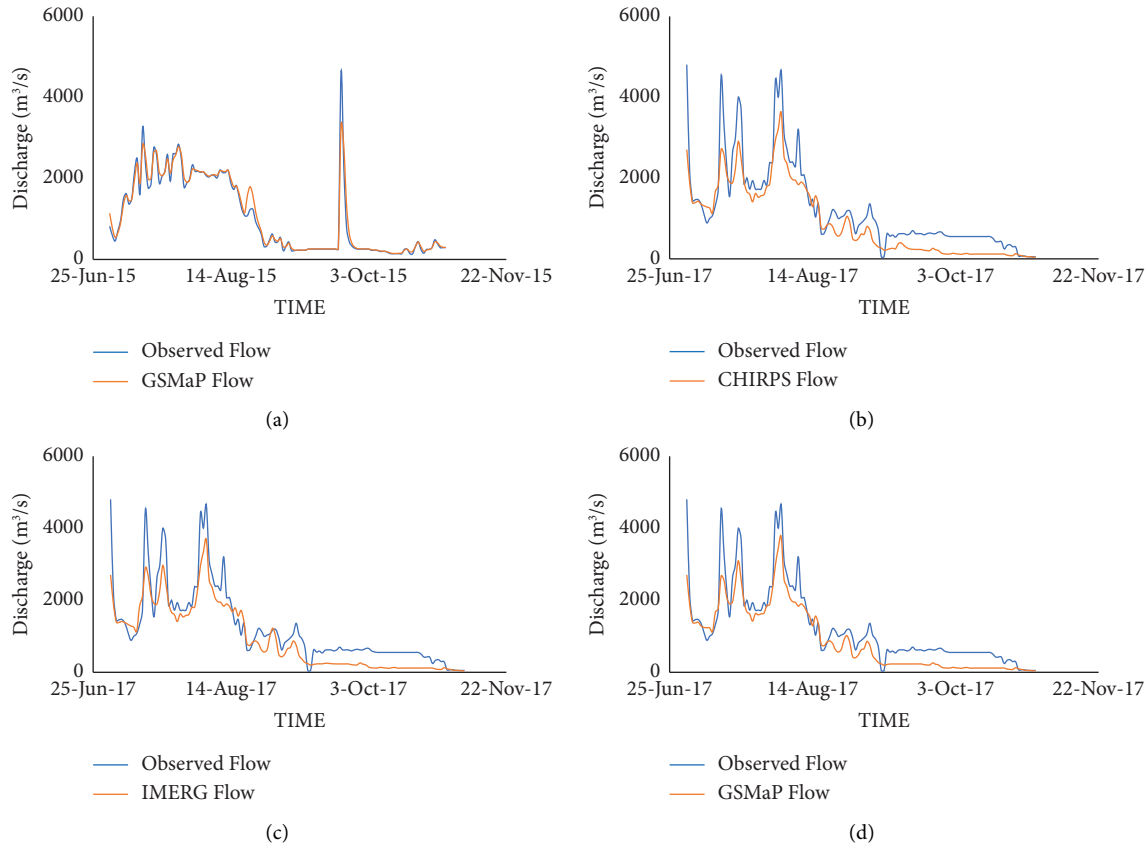

Figure 9: Graphical representations of calibration and validation scenario 2. (a) Calibration-GSMaP. (b) Validation CHIRPS. (c) Validation IMERG. (d) Validation GSMaP.

dataset to optimize the parameters and calibrate the model was better when compared with the CHIRPS precipitation model. A graphical presentation of scenario 2 is shown in Figure 9. It depicted a trend identical to scenario 1, but a bit improved simulation was observed in predicting low and high flows.

For the third calibration scenario, the statistical performance indicators R^2, NSE, and PBIAS for model calibration were observed at 0.92, 0.91, and −0.11, respectively, which exhibited excellent performance of this model according to the calibration rating described by [52]. The R^2 of the GSMaP, IMERG, and CHIRPS datasets were 0.87,

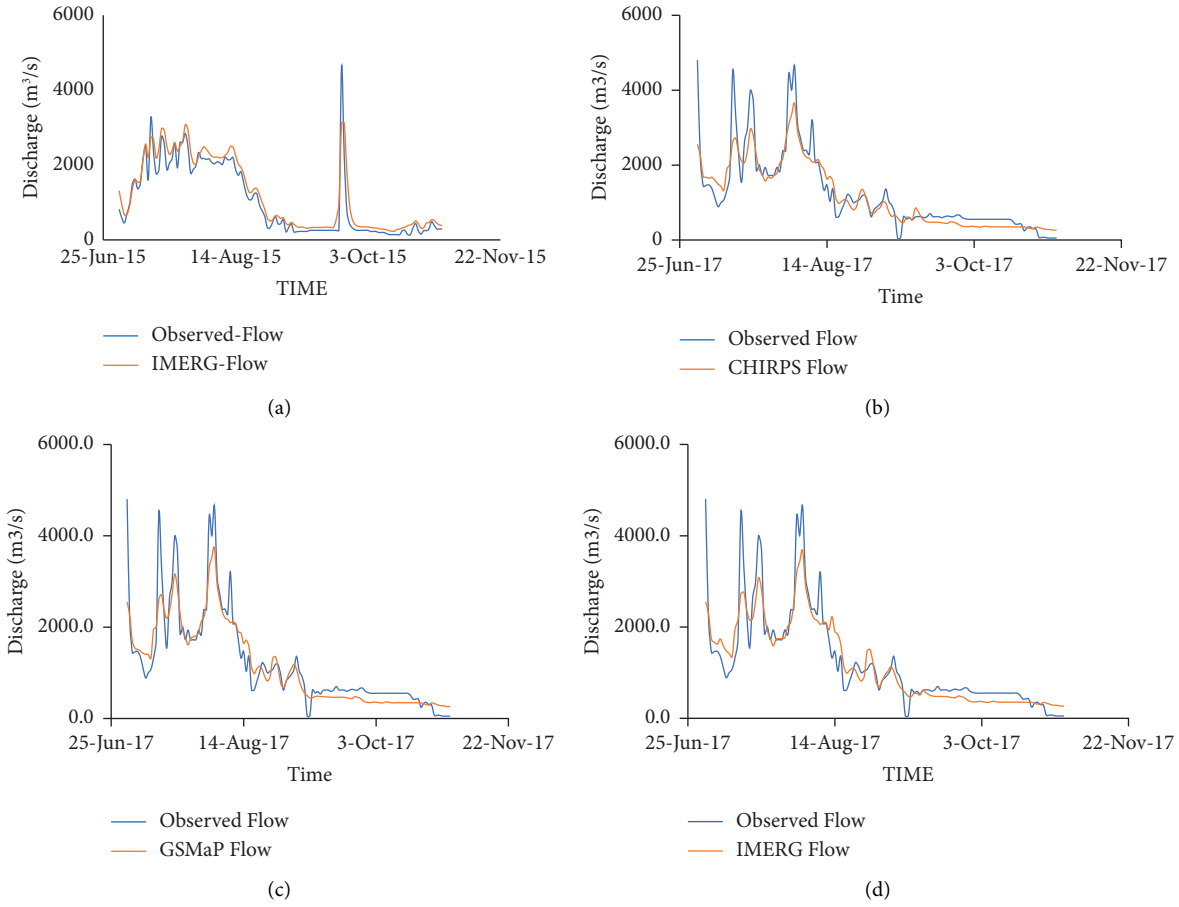

Figure 10: Graphical representations of calibration and validation scenario 3. (a) Calibration-IMERG. (b) Validation CHIRPS. (c) Validation GSMaP. (d) Validation CHIRPS.

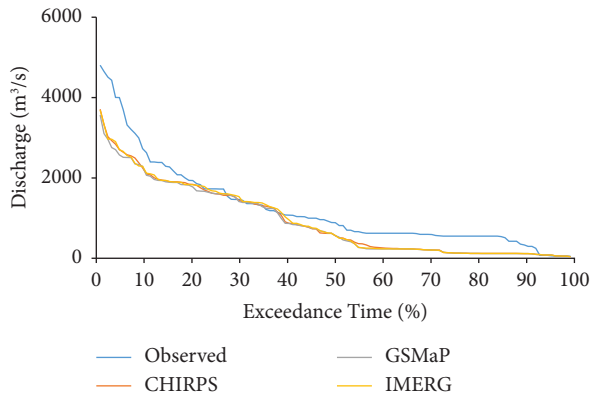

Figure 11: Assessment of the used SPPs in terms of hydraulic signature through FDC.

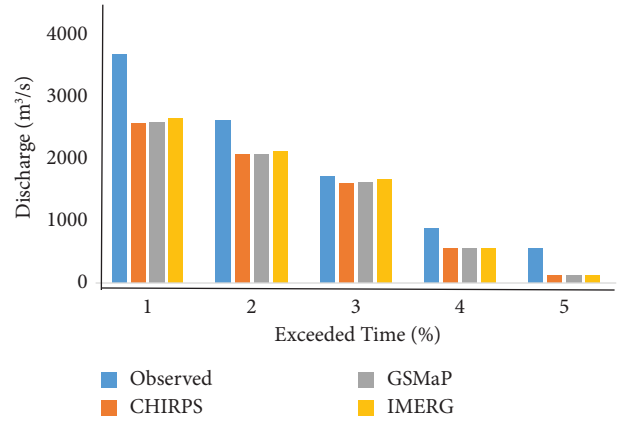

Figure 12: Assessment of the used SPPs in the term dependable flows.

0.85, and 0.84, respectively, which depicts better GSMaP product performance for the third scenario also. A graphical presentation of this scenario, Figure 10, shows identical performance in forecasting low and high flows.

It was noted that GSMaP outerperformed in terms of parameter optimization and fine-tuning of the IFAS model during the calibration procedure with R^2, NSE, and PBIAS values of 0.97, 0.96, and −0.03, respectively. For PBIAS evaluation, GSMaP produced a lower value of −0.03, compared to the other two products, CHIRPS and IMERG simulated moderately higher values of −0.11 and −0.16, respectively. IMERG and CHIRPS were rated in the second and third positions for performance evaluation of model calibration. In the case of the application and validation of

the hydrological model for the high monsoon flood of 2017, GSMaP outperformed in each scenario. Overall, the hydrological performance of GSMaP was more satisfactory than that of IMERG and CHIRPS, IMERG was ranked second, while the CHIRPS exhibited a lower performance.

4.5. Hydrological Signature-Based Assessment. The hydrological performance of all selected satellite precipitation datasets was evaluated through FDC, in which daily observed stream flows were taken as the baseline and the variation in simulated flow was determined. The FDC results displayed that the selected satellite dataset has relatively inferior performance in capturing extreme flooding conditions. While considering the medium flow, all datasets showed excellent performance in the range of 20% to 40% exceedance time, as displayed in Figure 11.

Similarly, these precipitation datasets do not yield satisfactory results for the simulation of low flows. For all precipitation datasets at the catchment outlet stage, an exceedance flow analysis was used to estimate the dependable flow exceedance of Q5, Q10, Q25, Q50, and Q70. Q5 denotes a flow that exceeds 5% of the analysis time, and so forth. Extreme flood events are revealed by 5% and 10% stream flows, while 50% dependability designates the median flow, 70% dependable flow resembles the water availability for agriculture, and higher dependable flows correspond to the water availability for domestic supplies. The performances of SPPs to generate high, medium, and low flows was analyzed through these dependable flows. It was found that all SPPs data sets' performance was lower, corresponding to Q5 and Q70. The SPPs datasets can generate medium flow in the range of Q25-Q50 Figure 12.

5. Conclusion

The present study evaluated three high-resolution multi-satellite precipitation estimation products statistically and hydrologically in the Chenab River catchment. The consistency of rain gauge data observed by PMD was examined by double mass analysis. Numerous statistical indicators were applied at daily, monthly, and seasonal scales to detect and quantify errors associated with these products. Three different calibration scenarios were established for the hydrological assessment to analyze the satellite precipitation datasets. A sensitivity analysis was performed to study the most sensitive parameters of the distributed IFAS model. The hydrological signature was used to assess the potential of satellite products to generate high, medium, and low flows. The existence of about 62 percent of the catchment area in Indian-held Kashmir and the occurrence of only four gauging stations in the rest of the catchment area are the major limitations of the study towards hydrological and statistical assessment of the satellite products in the study area, respectively. From the findings of this study, it was observed as follows:

(1) PMD rain gauge-based precipitation data are consistent and can be used for the assessment of satellite-based precipitation datasets.

(2) Statistical evaluation revealed that the efficacy of GSMaP has been better, while CHIRPS showed more biases. The performance of SPPs improved at 10-daily and monthly time scales than at the daily time scale. Higher values of uncertainties (bias and RMSE) were observed during the monsoon season than during the western disturbances. Missed and false alarms were the main errors associated with SPPs due to spatial mobility and the sudden bursting of clouds, specifically during the monsoon season.

(3) The stativity analysis revealed that the aquifer tank parameters were found to be the most sensitive. The base flow coefficient (AGD) was found to be the most sensitive parameter in calibrating the IFAS model to simulate flows using SPPs.

(4) The model calibration and validation scenarios indicated that the GSMaP precipitation dataset has better capability to calibrate and validate the model compared to IMERG and CHIRPS, with the highest R^2, NSE and lower PBIAS values. It was also observed that the SPPs have relatively poor performance in capturing extreme flooding events. While considering the medium flows, in the range of 20%–40% exceedance time, all datasets showed excellent performance.

Findings of this study suggested that direct utilizations of satellite-based precipitation products were not promising at daily scales and bias correction is recommended. For flood modeling, the hydrological IFAS model should be calibrated based on peak flow, considering the combination of statistical and error indicators. Further studies may be carried out to assess the effectiveness of the available sensitivity analysis techniques in this study area.

Acronyms

SPPs:	Satellite precipitation products
IMERG:	Integrated Multi-satellite Retrieval for GPM
GSMaP:	Global Satellite Mapping of Precipitation
CHIRPS:	Climate Hazards Group Infrared Precipitation with Station
DMC:	Double mass curve
POD:	Probability of detection
CSI:	Critical success index
FAR:	False alarm ratio
CC:	Correlation coefficient
RMSE:	Root mean square error
B:	Bias
IFAS:	Integrated Flood Analysis System
FDC:	Flow duration curve
R^2:	Coefficient of determination
AGD:	Base flow coefficient
NSE:	Nash–Sutcliffe efficiency
PBIAS:	Percentage bias
PMD:	Pakistan Metrological Department
WMO:	World Meteorological Organization
FFD:	Flood forecasting division
JAXA:	Japan Aerospace Exploration Agency

NASA: National Aeronautics and Space Administration
PMW: Passive microwave
IR: Infrared
CPC: Climate prediction center
GPM: Global precipitation measurement
CCD: Cold cloud duration
DEM: Digital elevation model
ISCGM: International Steering Committee for Global Mapping
DSMW: Digital soil map of the world
FAO: Food and Agriculture Organization
PWRI-DHM: Public Works Research Institute distributed hydrological model
IWRM: Integrated water resources management
MPIs: Model performance indicators.

Data Availability

The data used to support the findings of this study are available from the corresponding author upon request.

Conflicts of Interest

The authors declare that they have no conflicts of interest.

Acknowledgments

The authors are grateful to the Center of Excellence in Water Resource Engineering for support in conducting this study. The authors are also thankful to PMD/FFD and satellite organizations for the data used in the study.

References

[1] M. T. Mendoza and R. Schwarze, "Sequential disaster forensics: a case study on direct and socio-economic impacts," *Sustainability*, vol. 11, no. 21, pp. 1–20, 2019.

[2] A. Mishra, A. Alnahit, and B. Campbell, "Impact of land uses, drought, flood, wildfire, and cascading events on water quality and microbial communities: a review and analysis," *Journal of Hydrology*, vol. 596, Article ID 125707, 2021.

[3] F. Dottori, W. Szewczyk, J. C. Ciscar et al., "Increased human and economic losses from river flooding with anthropogenic warming," *Nature Climate Change*, vol. 8, no. 9, pp. 781–786, 2018.

[4] A. Mishra, S. Mukherjee, B. Merz et al., "An overview of flood concepts, challenges, and future directions," *Journal of Hydrologic Engineering*, vol. 27, no. 6, pp. 1–30, 2022.

[5] S. Janjua, I. Hassan, S. Muhammad, S. Ahmed, and A. Ahmed, "Water management in Pakistan's Indus basin: challenges and opportunities," *Water Policy*, vol. 23, no. 6, pp. 1329–1343, 2021.

[6] A. R. Iqbal, "Environmental issues of Indus River Basin: an analysis," *Institute for Strategic Studies, Research & Analysis (ISSRA)*, vol. 5, no. 1, National Defence University, Islamabad, Pakistan, 2013.

[7] Federal Communications Commission, "Government of pakistan ministry of water resources," Annual Flood Report 2017, pp. 1–118, Federal Communications Commission, Washington, DC, USA, 2017.

[8] J. Pancawati, S. Nurisjah, and B. Pramudya, "Application of tank model for ungauged reservoir management: a case of situ cipondoh, tangerang Indonesia," *Journal of Environment and Earth Science*, vol. 9, no. 1, pp. 52–61, 2019.

[9] M. Aslam, "Flood management current state, challenges and prospects in Pakistan: a review," *Mehran University Research Journal of Engineering and Technology*, vol. 37, no. 2, pp. 297–314, 2018.

[10] M. S. Shrestha, M. R. Khan, N. Wagle, Z. Ahmad Babar, V. R. Khadgi, and S. Sultan, *Review of Hydrometeorological Monitoring and Forecasting System for Floods in the Indus Basin in Pakistan*, Elsevier Inc, Amsterdam, Netherlands, 2019.

[11] S. Sorooshian, A. Aghakouchak, P. Arkin et al., "Advanced concepts on remote sensing of precipitation at multiple scales," *Bulletin of the American Meteorological Society*, vol. 92, no. 10, pp. 1353–1357, 2011.

[12] A. U. Rehman, F. Chishtie, W. A. Qazi, S. Ghuffar, I. Fatima, and K. Fatima, "Evaluation of three-hourly TMPA rainfall products using telemetric rain gauge observations at lai nullah basin in islamabad, Pakistan," *Remote Sensing*, vol. 10, no. 12, p. 2040, 2018.

[13] Y. Zhang, A. Sun, H. Sun et al., "Error adjustment of TMPA satellite precipitation estimates and assessment of their hydrological utility in the middle and upper yangtze River Basin, China," *Atmospheric Research*, vol. 216, pp. 52–64, 2019.

[14] C. Miao, H. Ashouri, K. L. Hsu, S. Sorooshian, and Q. Duan, "Evaluation of the PERSIANN-CDR daily rainfall estimates in capturing the behavior of extreme precipitation events over China," *Journal of Hydrometeorology*, vol. 16, no. 3, pp. 1387–1396, 2015.

[15] B. Yong, Y. Hong, L. L. Ren et al., "Assessment of evolving TRMM-based multisatellite real-time precipitation estimation methods and their impacts on hydrologic prediction in a high latitude basin," *Journal of Geophysical Research: Atmospheres*, vol. 117, no. 9, 2012.

[16] D. B. Michelson, "Systematic correction of precipitation gauge observations using analyzed meteorological variables," *Journal of Hydrology*, vol. 290, no. 3-4, pp. 161–177, 2004.

[17] P. S. Roy, M. D. Behera, and S. K. Srivastav, "Satellite remote sensing: sensors, applications and techniques," *Proceedings of the National Academy of Sciences India Section A - Physical Sciences*, vol. 87, no. 4, pp. 465–472, 2017.

[18] K. J. Beven and H. L. Cloke, "Comment on 'Hyperresolution Global Land Surface Modeling: meeting a Grand Challenge for Monitoring Earth's Terrestrial Water' by Eric F. Wood et Al," *Water Resources Research*, vol. 48, no. 1, pp. 1–10, 2012.

[19] K. Yan, G. Di Baldassarre, D. P. Solomatine, and G. J. P. Schumann, "A review of low-cost space-borne data for flood modelling: topography, flood extent and water level," *Hydrological Processes*, vol. 29, no. 15, pp. 3368–3387, 2015.

[20] Z. N. Musa, I. Popescu, and A. Mynett, "A review of applications of satellite SAR, optical, altimetry and DEM data for surface water modelling, mapping and parameter estimation," *Hydrology and Earth System Sciences*, vol. 19, no. 9, pp. 3755–3769, 2015.

[21] M. Masood, A. S. Shakir, A. H. Azhar, G. Nabi, and H. U. Rehman, "Assessment of real time, multi-satellite precipitation products under diverse climatic and topographic conditions," *Asia-Pacific Journal of Atmospheric Sciences*, vol. 56, no. 4, pp. 577–591, 2019.

[22] J. Shi, F. Yuan, C. Shi et al., "Statistical evaluation of the latest GPM-era IMERG and GSMaP satellite precipitation products in the yellow river source region," *Water (Switzerland)*, vol. 12, no. 4, pp. 1006–1023, 2020.

[23] N. Saddique, M. Muzammil, I. Jahangir et al., "Hydrological evaluation of 14 satellite-based, gauge-based and reanalysis precipitation products in a data-scarce mountainous catchment," *Hydrological Sciences Journal*, vol. 67, no. 3, pp. 436–450, 2022.

[24] G. Villarini, W. F. Krajewski, and J. A. Smith, "New paradigm for statistical validation of satellite precipitation estimates: application to a large sample of the TMPA 0.25° 3-hourly estimates over Oklahoma," *Journal of Geophysical Research*, vol. 114, no. 12, pp. 12106–12112, 2009.

[25] B. Nijssen and D. P. Lettenmaier, "Effect of precipitation sampling error on simulated hydrological fluxes and states: anticipating the global precipitation measurement satellites," *Journal of Geophysical Research: Atmospheres*, vol. 109, no. 2, pp. 1–15, 2004.

[26] J. R. McCollum, R. Witold, R. R. Krajewski, and M. B. Ba, "Evaluation of biases of satellite rainfall estimation algorithms over the continental United States," *Journal of Applied Meteorology*, vol. 41, no. 11, pp. 1065–1080, 2002.

[27] F. L. Conti, K. L. Hsu, L. V. Noto, and S. Sorooshian, "Evaluation and comparison of satellite precipitation estimates with reference to a local area in the mediterranean sea," *Atmospheric Research*, vol. 138, pp. 189–204, 2014.

[28] M. Masood, G. Nabi, M. Babur, A. H. Azhar, and M. Kaleem Ullah, "Disintegration of uncertainties associated with real-time multi-satellite precipitation products in diverse topographic and climatic area in Pakistan," *Journal of Mountain Science*, vol. 18, no. 3, pp. 716–734, 2021.

[29] Y. Tuo, Z. Duan, M. Disse, and G. Chiogna, "Evaluation of precipitation input for swat modeling in alpine catchment: a case study in the adige River Basin (Italy)," *Science of the Total Environment*, vol. 573, pp. 66–82, 2016.

[30] T. M. Sharannya, N. Al-Ansari, S. Deb Barma, A. Mahesha, and A. Mahesha, "Evaluation of satellite precipitation products in simulating streamflow in a humid tropical catchment of India using a semi-distributed hydrological model," *Water (Switzerland)*, vol. 12, no. 9, p. 2400, 2020.

[31] M. Umer, H. F. Gabriel, S. Haider, A. Nusrat, M. Shahid, and M. Umer, "Application of precipitation products for flood modeling of transboundary River Basin: a case study of Jhelum basin," *Theoretical and Applied Climatology*, vol. 143, no. 3-4, pp. 989–1004, 2021.

[32] R. H. McCuen, "The role of sensitivity analysis in hydrologic modeling," *Journal of Hydrology*, vol. 18, no. 1, pp. 37–53, 1973.

[33] K. K. Yilmaz, H. V. Gupta, and T. Wagener, "A process-based diagnostic approach to model evaluation: application to the NWS distributed hydrologic model," *Water Resources Research*, vol. 44, no. 9, pp. 1–18, 2008.

[34] K. Sawicz, T. Wagener, M. Sivapalan, P. A. Troch, and G. Carrillo, "Catchment classification: empirical analysis of hydrologic similarity based on catchment function in the eastern USA," *Hydrology and Earth System Sciences*, vol. 15, no. 9, pp. 2895–2911, 2011.

[35] I. K. Westerberg and H. K. McMillan, "Uncertainty in hydrological signatures," *Hydrology and Earth System Sciences*, vol. 19, no. 9, pp. 3951–3968, 2015.

[36] F. Mendonça, R. P. Oliveira, and F. F. Mauad, "Lumped versus distributed hydrological modeling of the jacaré-guaçu basin, Brazil," *Journal of Environmental Engineering*, vol. 144, no. 8, Article ID 04018056, 2018.

[37] H. Brirhet and L. Benaabidate, "Comparison of two hydrological models (lumped and distributed) over A pilot area of the issen watershed in the souss basin, Morocco," *European Scientific Journal*, vol. 12, no. 18, p. 347, 2016.

[38] A. Sugiura, S. Fujioka, S. Nabesaka, M. Tsuda, and Y. Iwami, "Development of a flood forecasting system on the upper Indus catchment using IFAS," *Journal of Flood Risk Management*, vol. 9, no. 3, pp. 265–277, 2016.

[39] A. Shahzad, H. F. Gabriel, S. Haider, A. Mubeen, and M. J. Siddiqui, "Development of a flood forecasting system using IFAS: a case study of scarcely gauged Jhelum and Chenab River basins," *Arabian Journal of Geosciences*, vol. 11, no. 14, p. 383, 2018.

[40] A. Aziz and S. Tanaka, "Regional parameterization and applicability of integrated flood analysis system (IFAS) for flood forecasting of upper-middle Indus river classification of hydrological models," *Pakistan Journal of Meterorology*, vol. 8, no. 15, pp. 21–38, 2010.

[41] M. Miyamoto, M. Ono, S. Nabesaka, T. Okazumi, and Y. Iwami, "Applicability of a flood forecasting method utilizing global satellite information to an insufficiently-gauged River Basin: A case of a River Basin in the Philippines," in *Proceedings of the 11th International Conference on Hydroinformatics*, New York, NY, USA, August 2014.

[42] H. Ishak, M. D. Nor, L. M. Sidek et al., "Flood forecasting and early warning system for dungun river basin," *IOP Conference Series: Earth and Environmental Science*, vol. 16, no. 1, 2013.

[43] R. Awan, "Pakistan flood Management.Pdf (Application/Pdf object)," *Mainstream*, vol. 1, pp. 1–4, 2003.

[44] M. Riaz, A. Aziz, and S. Hussain, "Flood forecasting of an ungauged trans-boundary Chenab River Basin using distributed hydrological model integrated flood analysis system (IFAS)," *Pakistan Journal of Meteorology*, vol. 13, no. 26, pp. 51–62, 2017.

[45] G. J. Huffman, D. T. Bolvin, D. Braithwaite et al., *Algorithm Theoretical Basis Document (ATBD) Version 5.2 for the NASA Global Precipitation Measurement (GPM) Integrated Multi-satellitE Retrievals for GPM (I-MERG)*, GPM Project, Greenbelt, MD, USA, 2019.

[46] S. Sharma, Y. Chen, X. Zhou et al., "Evaluation of GPM-era satellite precipitation products on the southern slopes of the central himalayas against rain gauge data," *Remote Sensing*, vol. 12, no. 11, p. 1836, 2020.

[47] C. Funk, P. Peterson, M. Landsfeld et al., "The climate hazards infrared precipitation with stations - a new environmental record for monitoring extremes," *Scientific Data*, vol. 2, p. 150066, 2015.

[48] M. Masood, A. S. Shakir, and H. U. Rehman, "Assessment of GPM based integrated multi-satellite retrievals under diverse climatic and topographic conditions in Pakistan," vol. 23, pp. 17–29, 2018.

[49] T. Sugiura, K. Fukami, and H. Inomata, "Development of integrated flood analysis system (IFAS) and its applications," in *Proceedings of the World Environmental and Water Resources Congress*, vol. 316, Pittsburgh, PA, USA, May 2008.

[50] S. Sutikno, Y. L. Handayani, M. Fauzi, Fitriani, and A. Kurnia, "Hydrologic modelling using TRMM-based rainfall products for flood analysis," *MATEC Web of Conferences*, vol. 101, pp. 2–6, 2017.

[51] A. Aziz and S. Tanaka, "Regional parameterization and applicability of integrated flood analysis system (IFAS) for flood forecasting of upper-middle Indus River classification of hydrological models," *Pakistan Journal of Meterorology*, vol. 8, no. 15, pp. 21–38, 2010.

[52] D. N. Moriasi, D. J. G. Arnold, M. W. Van Liew, R. L. Bingner, R. D. Harmel, and T. L. Veith, "Model evaluation guidelines

for systematic quantification of accuracy in watershed simulations," *Transactions of the ASABE*, vol. 50, no. 3, pp. 885–900, 2007.

[53] G. Tang, M. P. Clark, S. M. Papalexiou, Z. Ma, and Y. Hong, "Have satellite precipitation products improved over last two decades? A comprehensive comparison of GPM IMERG with nine satellite and reanalysis datasets," *Remote Sensing of Environment*, vol. 240, Article ID 111697, 2020.

[54] S. Ning, S. Fan, P. Udmale, J. Jin, B. Raj Thapa, and H. Ishidaira, "Error analysis and evaluation of the latest GSMap and IMERG precipitation products over eastern China," *Advances in Meteorology*, vol. 2017, Article ID 1803492, 16 pages, 2017.

[55] A. Nusrat, H. F. Gabriel, S. Haider, and M. Siddique, "Sensitivity analysis and optimization of land use/cover and aquifer parameters for improved calibration of hydrological model," *Mehran University Research Journal of Engineering and Technology*, vol. 41, no. 2, pp. 21–34, 2022.